NUMERICAL AND ANALYTICAL APPROACH FOR SAKIADIS RHEOLOGY OF GENERALIZED POLYMERIC MATERIAL WITH MAGNETIC FIELD AND HEAT SOURCE/SINK

Muhammad AWAIS[1] , Saeed Ehsan AWAN [2] , Aqsa[3] , Nimra MUQADDASS[1] , Saeed Ur REHMAN[2] , Muhammad Asif Zahoor RAJA [2,*]

[1]Department of Mathematics, COMSATS University Islamabad, Attock Campus, Attock, Pakistan

[2]Department of Electrical Engineering, COMSATS University Islamabad, Attock Campus, Pakistan

[3]Department of Mathematics, Quaid-i-Azam University Islamabad, Pakistan
[*] Corresponding author; E-mail: muhammad.asif@ciit-attock.edu.pk

Abstract: *In this analysis, Sakiadis rheology of the generalized polymeric material has been presented with magnetic field and heat source/sink. Convective heating process with thermal radiations have been incorporated. Mathematical modelling has been performed for the conversion of physical problem into set of nonlinear equations. Suitable transformations have been employed in order to convert the derived PDEs into set of nonlinear ODEs. Analytical as well as finite difference method based numerical solutions for the velocity and temperature profiles are computed. Graphical and numerical illustrations have been presented in order to analyze the behavior of involved physical quantities. Error analysis for the nonlinear system has been presented in order to show the validity of the obtained results. Bar charts have been plotted to present the heat flux analysis. Tabular values of local Nusselt number are computed for the involved key parameters. Heat transfer rates against magnetic and porosity effects found to be decreased since magnetic field and porosity retard the molecular movement of the fluid particles. This controlling property of magnetic field and porosity effects have application in MHD power generation, electromagnetic casting of metals, MHD ion propulsion etc. Moreover internal heat generation and absorption effects have opposite effects on the fluid temperature.*

Key words*: maximum 10 Generalized polymeric material, Oldroyd-B model; Sakiadis flow; Heat source/ sink; Magnetic field.*

1. Introduction

Fluid flow problem induced due to moving surfaces with heat transfer analysis under the application of magneto-hydrodynamics (MHD) are one of the useful problems in fluid mechanics due to their relevance with engineering and industry, for-instance, in metal extrusion, wire coating, fiber spinning, glass blowing, manufacturing, sheeting stuff, i.e., paper, fiber and metallic sheets, and in the process of polymer extrusion in which the sheet experiences the stretching phenomenon in order to acquire the preferred thickness [1-5]. In these applications, the value of the final outcome strongly depends upon the cooling rate, so in such processes, the mechanism of cooling rate lead to gain the final product of desired features [6-7]. Sakiadis [8-9] present the seminal work on the boundary layer flows and successfully introduce to several engineering and industrial applications. Later on, researchers investigated in applied mathematics and physics domains have analyzed his ideas and utilized them effectively to provide the reliable solution of several new scientific problems, such as Zierep and Fetecau [10] investigate in Rayleigh-Stokes problem involving the Maxwell fluid. Jamil et al. [11] in fluidics problems based on unsteady helical fluid flow. He considered the Oldroyd-B fluid model and presented the relaxation/ retardation time properties, Tan and Masuoka [12] presented the stability analyses for the Maxwell fluid problem with porous medium in the presence of thermal heating, Nadeem et al. [13] provide the Homotopy analysis based results for the boundary layer flow in the region of the stagnation point towards a stretching sheet, Hayat et al. [14] computed the thermal radiation as well as Joule heating dynamics for the MHD flow involving the Oldroyd-B fluid in the scenarios of the thermophoresis phenomenon. Malik et al. [15] investigated the model based on hydromagnetic three-dimensional Maxwell fluid flow problem, Hayat et al. [16] analyze the dynamics of mixed convective 3D flow problem involving the upper-convective Maxwell fluid in the presence of magnetic field. Mehmood et al. [17] presented numerical treatment for micropolar Casson fluid over a stretching sheet, Ramesh et al. [18] investigated in nanofluid flow problem for heat generation on Maxewell fluid, Mehmood et al. [19] analyzed the Jeffery nano fluid impinging obliquely over a stretched plate, Kumar [20] computed the effect of flow of Oldroyd B nanofluid with thermal radiation, Rana et al. [21] provided the numerical treatment on non-Newtonian flow with non-linear thermal radiation problems, Awais el al. [22] study the Sakeidis flow of polymeric nanoliquids and Generally, many studies have been reported recently to analyze the physical behaviour of fluid mechanics problems, [23-27] and reference in them.

In this investigation we have extended the problem of fluid flow over a moving surface into new directions. We have considered the heat transfer analysis for the Sakiadis flow for the rheology of an Oldroyd-B fluid. Mathematical modelling of the momentum equation reveals the occurrence of generalized magnetic field term. The fluid dynamics in a porous medium under the application of internal heat generation/ absorption and thermal radiation effects are analyzed. Analytical and numerical treatment have been performed for the momentum and energy dynamics by exploiting the strength of Homotopy analysis method [28-33] and numerical procedure of finite difference scheme. Error analysis for the velocity and temperature profiles are presented to show the validity of the obtained results. Numerical and graphical illustration in term of Tables and plots are presented to study the effect of rheology by varying the involved physical quantities.

2. Mathematical Formulation

Consider the rheology of an Oldroyd-B model (a subclass of rate type fluid model) over a wall. Sakiadis flow situation has been considered within a porous medium. Magnetic field of strength B_0 is applied along a transverse direction in order to predict the magneto-hydrodynamics as shown in Fig. 1. Convective heat process has been considered to study the thermal properties at the wall and within the system.

The mathematical equations [32] governing the flow with internal heat generation/ absorption properties are

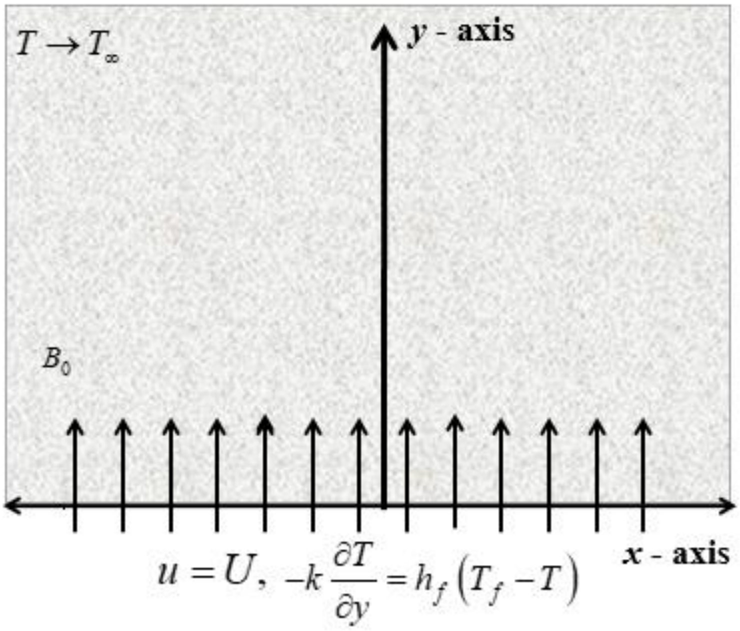

Fig. 1: Physical model.

$\operatorname{div}\mathbf{V} = 0,$	(1)
$\rho\dfrac{D\mathbf{V}}{Dt} = -\nabla p + \operatorname{div}\mathbf{S},$	(2)
$\left(1+\lambda_1\dfrac{D}{Dt}\right)S = \mu\left(1+\lambda_2\dfrac{D}{Dt}\right)A_1,$	(3)
$\dfrac{Da_i}{Dt} - \dfrac{\partial a_i}{\partial t} - u_r a_{i,r} + u_{i,r}a_r = 0,$	(4)
$\rho c_p\dfrac{d\mathbf{T}}{dt} = k^*\nabla^2\mathbf{T} + \bar{q},$	(5)

here the $\mathbf{V}$ represents the velocity field, fluid density ρ, stress tenser $\mathbf{S}$, Rivlin-Ericksen tenser $\mathbf{A}_1$ relaxation time effect λ_1, retardation time effect λ_2, dynamic viscosity μ and covariant derivative *D/Dt*. Simplifying equations (2-5) as:

$$u\frac{\partial u}{\partial x}+v\frac{\partial u}{\partial y}=-\lambda_1\left(u^2\frac{\partial^2 u}{\partial x^2}+v^2\frac{\partial^2 u}{\partial y^2}+2uv\frac{\partial u}{\partial x\partial y}\right)-\left(\frac{\sigma B^2{}_0}{\rho}+\frac{\nu}{k}\right)\left(u+\lambda_1 v\frac{\partial u}{\partial y}\right)$$
$$+\nu\left\{\frac{\partial^2 u}{\partial y^2}+\lambda_2\left(u\frac{\partial^3 u}{\partial x\partial y^2}+v\frac{\partial^3 u}{\partial y^3}-\frac{\partial u}{\partial x}\frac{\partial^2 u}{\partial y^2}-\frac{\partial u}{\partial y}\frac{\partial^2 v}{\partial y^2}\right)\right\}, \quad (6)$$

$$u\frac{\partial T}{\partial x}+v\frac{\partial T}{\partial y}=\alpha_m\frac{\partial^2 T}{\partial z^2}-\frac{1}{\rho C_p}\frac{\partial q_r}{\partial y}+\frac{Q_0}{\rho C_p}(T-T_\infty). \quad (7)$$

It is noted that for $\lambda_2=0$, the results for Maxwell model can be deduced. Additionally, in case of $\lambda_1=\lambda_2=0$, one has a Newtonian fluid model results.

The subjected wall properties [22] are

$$u=U,\ v=0,\ -k\frac{\partial T}{\partial y}=h_f\left(T_f-T\right),\ \text{at } y=0,$$
$$u\to 0,\ v\to 0,\ T\to T_\infty.\qquad \text{as } y\to\infty, \quad (8)$$

here σ and T represent the electrical conductivity and temperature of the fluid, respectively. Furthermore, B_0, K, c_p, α_m, Q_0 are the magnetic field strength, porosity of medium, specific heat constant, thermal conductivity and internal heat generation or absorption parameter, respectively, while the radiative thermal flux quantity q_r is defined as $q_r=-(4\sigma^3/3k^*)\partial T^4/\partial y$. Making use of the following quantities

$$\eta=\sqrt{\frac{U}{\nu x}}\,y,\ u=Uf',\ v=-\frac{1}{2}\sqrt{\frac{\nu U}{x}}\left(f-\eta f'\right),\ \theta(\eta)=\frac{T-T_\infty}{T_{fW}-T_\infty}, \quad (9)$$

in equations (5-8), we get

$$f'''+\left(\frac{1}{2}\right)ff''-\frac{D_e}{2}\left(2ff'f''+\eta f'^2f''+f^2f'''\right)-M^2\left(f'-D_e\left(f-\eta f'\right)f''\right)$$
$$-Kf'+KD_e\left(ff''-\eta f'f''\right)+D_s\left(2\left(\eta f'f'''+\eta ff''''-ff'''\right)-ff''''-f''^2\right)=0, \quad (10)$$

$$\theta''+\Pr\left(\frac{1}{2}f\theta'+hs\theta\right)+\frac{4}{3}Rd\theta''=0, \quad (11)$$

along with the wall conditions

$$f(\eta)=0,\quad f'(\eta)=1,\quad \theta'(\eta)=-\gamma_1\left(1-\theta(\eta)\right),\ \text{at } \eta=0$$
$$f'(\eta)\to 0,\quad \theta(\eta)\to 0\qquad as\ \eta=\infty., \quad (12)$$

Note that in above equations $D_e = \lambda_1 U / 2x$ and $D_s = \lambda_2 U / 2x$ are representing the Deborah numbers, $M = \sqrt{\delta\beta_\circ^2 / \rho U}$ is the magnetic parameter, $K = \nu / kU$ is the porosity coefficient, $R_d = 16\delta^* T_\infty^3 / 3k'k^*$ is the radiation factor, $\Pr = \upsilon / \alpha_m$ is the Prandtl number, $hs = Q_\circ / U\rho C_p$ is the internal heat generation/absorption quantity. The quantity of physical interest are the thermal variation at wall " Nu_x " as given by

$$Nu_x = \frac{xq_w}{k(T_f - T_\infty)}, \tag{13}$$

in which q_w represents the wall heat flux as:

$$q_w = -k\left(\frac{\partial T}{\partial y}\right)_{y=0} + \left(q_r\right)_{y=0}. \tag{14}$$

In dimensionless form, above equations can be written as:

$$Nu_x / \mathrm{Re}_x^{1/2} = -\left(1 + \frac{4}{3}Rd\right)\theta'(0), \tag{15}$$

Solution techniques

Series solution: Homotopy analysis method (HAM) has been employed for solving equations (10-12). The initial guesses and linear operator for f and θ are selected as:

$$f_0(\eta) = 1 - e^{-\eta}, \qquad \theta_0(\eta) = \left(\frac{\gamma_1}{1+\gamma_1}\right)e^{-\eta}, \tag{16}$$

while the appropriate initial guesses are

$$f''' - f' = 0, \qquad \theta''' - \theta = 0, \tag{17}$$

Associated zeroth order problems are as follows

$$(1-p)L_f\left[f(\eta;p) - f_0(\eta)\right] = ph_f N_f\left[f(\eta;p)\right], \tag{18}$$

$$(1-p)L_\theta\left[\theta(\eta;p) - \theta_0(\eta)\right] = ph_\theta N_\theta\left[\theta(\eta;p), f(\eta;p)\right], \tag{19}$$

in which N_f and N_θ are nonlinear operators defined as

$$\mathbf{N}_f\left[f(\eta,p)\right]=\frac{\partial^3 f(\eta,p)}{\partial\eta^3}+\frac{1}{2}\left(f(\eta,p)\frac{\partial^2 f(\eta,p)}{\partial\eta^2}\right)-K\frac{\partial f(\eta,p)}{\partial\eta}$$
$$-\frac{De}{2}\left(\begin{array}{l}2f(\eta,p)\dfrac{\partial f(\eta,p)}{\partial\eta}\dfrac{\partial^2 f(\eta,p)}{\partial\eta^2}+\\ \eta\left(\dfrac{\partial f(\eta,p)}{\partial\eta}\right)^2\dfrac{\partial^2 f(\eta,p)}{\partial\eta^2}+\left(f(\eta,p)\right)^2\dfrac{\partial^3 f(\eta,p)}{\partial\eta^3}\end{array}\right)$$
$$-M^2\left(\begin{array}{l}\dfrac{\partial f(\eta,p)}{\partial\eta}-\\ De\left(f(\eta,p)-\eta\dfrac{\partial f(\eta,p)}{\partial\eta}\right)\dfrac{\partial^2 f(\eta,p)}{\partial\eta^2}\end{array}\right)+KDe\left(\begin{array}{l}f(\eta,p)\dfrac{\partial^2 f(\eta,p)}{\partial\eta^2}\\ -\eta\dfrac{\partial f(\eta,p)}{\partial\eta}\dfrac{\partial^2 f(\eta,p)}{\partial\eta^2}\end{array}\right)$$

$$+Ds\left(\begin{array}{l}2\left(\eta\dfrac{\partial f(\eta,p)}{\partial\eta}\dfrac{\partial^3 f(\eta,p)}{\partial\eta^3}+\eta\dfrac{\partial f(\eta,p)}{\partial\eta}\dfrac{\partial^4 f(\eta,p)}{\partial\eta^4}-\dfrac{\partial f(\eta,p)}{\partial\eta}\dfrac{\partial^3 f(\eta,p)}{\partial\eta^3}\right)\\ -f(\eta,p)\dfrac{\partial^4 f(\eta,p)}{\partial\eta^4}-\left(\dfrac{\partial^2 f(\eta,p)}{\partial\eta^2}\right)^2\end{array}\right), \quad (20)$$

$$\mathbf{N}_\theta\left[\theta(\eta,p)\right]=\frac{\partial^2\theta(\eta,p)}{\partial\eta^2}+\Pr\left(\frac{f(\eta,p)}{2}\frac{\partial\theta(\eta,p)}{\partial\eta}+hs\theta(\eta,p)\right)+\frac{4}{3}Rd\frac{\partial^2\theta(\eta,p)}{\partial\eta^2} \quad (21)$$

Using Taylor's series for expansion of $f(\eta,p)$ and $\theta(\eta,p)$, and considering that the resulting series are convergent at *.p=1.0* we get

$$f(\eta)=f_0(\eta)+\sum_{m=1}^{\infty}f_m(\eta),$$
$$\theta(\eta)=\theta_0(\eta)+\sum_{m=1}^{\infty}\theta_m(\eta). \quad (22)$$

Where

$$f_m(\eta)=\left[\frac{1}{m!}\frac{\partial^m f(\eta;p)}{\partial p^m}\right]_{p=0}{}'\theta_m(\eta)=\left[\frac{1}{m!}\frac{\partial^m\theta(\eta;p)}{\partial p^m}\right]_{p=0} \quad (23)$$

The problems of m^{th} order given as:

$$L_f\left[f_m(\eta)-\chi_m f_{m-1}(\eta)\right]=\hbar_f R_m^f(\eta), \quad (24)$$

$$L_\theta\left[\theta_m(\eta)-\chi_m\theta_{m-1}(\eta)\right]=\hbar_f R_m^\theta(\eta), \quad (25)$$

and the nonlinear operators are

$$
\begin{aligned}
R_m^f(\eta) = {} & f'''_{m-1} + \frac{1}{2}\sum_{k=0}^{m-1}\left[f_{m-1-k} f''_k\right] - De\sum_{k=0}^{m-1} f_{m-1-k}\sum_{l=0}^{k}\left[f'_{k-l} f''_l\right] - \frac{De}{2}\eta\sum_{k=0}^{m-1} f'_{m-1-k}\sum_{l=0}^{k}\left[f'_{k-l} f''_l\right] \\
& - \frac{De}{2}\sum_{k=0}^{m-1} f_{m-1-k}\sum_{l=0}^{k}\left[f_{k-l} f'''_l\right] - M^2 f'_{m-1} + M^2 De\sum_{k=0}^{m-1}\left[f_{m-1-k} f''_k\right] - M^2 De\eta\sum_{k=0}^{m-1}\left[f_{m-1-k} f''_k\right] \\
& + KDe\sum_{k=0}^{m-1}\left[f_{m-1-k} f''_k - \eta f'_{m-1-k} f''_k\right] + 2Ds\sum_{k=0}^{m-1}\left[\eta f''_{m-1-k} f'''_k + \eta f'_{m-1-k} f''''_k - f'_{m-1-k} f'''_k\right] \\
& - Kf'_{m-1} - Ds\sum_{k=0}^{m-1}\left[f_{m-1-k} f''''_k + f''_{m-1-k} f''_k\right],
\end{aligned} \tag{26}
$$

$$
R_m^\theta(\eta) = \theta''_{m-1} + \frac{4}{3}Rd\,\theta''_{m-1} + \Pr hs\,\theta_{m-1} + \Pr\left(\sum_{k=0}^{m-1}\left[\frac{1}{2}\theta'_{m-1-k} f_k\right]\right) \tag{27}
$$

$$
\chi_m = \begin{cases} 0, & m \le 1, \\ 1, & m > 1. \end{cases} \tag{28}
$$

Numerical Solution

System model represented by equations (10-12) are discretized using the forward, backward and central difference formula based on 5 point stencils [34-36].

For velocity profile $f(\eta)$, the discretization formulas are given as

$$
f'(\eta) = \frac{-25f(\eta+0h) + 48f(\eta+1h) - 36f(\eta+2h) + 16f(\eta+3h) - 3f(\eta+4h)}{12h^1} \tag{29}
$$

$$
f''(\eta) = \frac{35f(\eta+0h) - 104f(\eta+1h) + 114f(\eta+2h) - 56f(\eta+3h) + 11f(\eta+4h)}{12h^2} \tag{30}
$$

$$
f'''(\eta) = \frac{-5f(\eta+0h) + 18f(\eta+1h) - 24f(\eta+2h) + 14f(\eta+3h) - 3f(\eta+4h)}{2h^3} \tag{31}
$$

Accordingly, the discretization formula for $\theta(\eta)$ are constructed similarly. With the help of discretization formula, the system equation (10-12) is transformed into system of nonlinear algebraic equations with are tackled numerically up to the tolerance level of 10^{-6}.

Error analysis

The set of equations (10-11) along with wall conditions (12) are coupled and highly nonlinear. Therefore, error analysis has been performed in order to get the validated results. We have prepared Figs. 2 and 3 which show the error in velocity and temperature profiles. These plots show that error in the computations are very much negligible.

Rheological results

It is noted that system of nonlinear equations (10-12) contains several physical and rheological quantities involving Deborah numbers, magnetic parameter, internal heat generation/ absorption quantity, wall convection parameter etc. Therefore, we have prepared Figs. (4-12) and Table 1 showing the behavior of the involved parameters on the velocity and temperature profiles. Fig. 4 and 5 presents the heat transfer rate for different values of magnetic parameter *M* and porosity parameter *K*. Front bar shows the results of Propane whereas back bar presents the results of Ethylene glycol. It is observed that heat transfer rate decreases in both case when the magnetic parameter and the porosity parameter are increased. Figs 6 and 7 are prepared to show the effects of Deborah numbers (*De* and *Ds*) on the flow field. It is observed that velocity profile and its associated boundary layer thickness decreases as values of Deborah number *De* gets higher but for the case of *Ds* velocity profile declines. Small values of Deborah numbers (*De*, *Ds* <<1) signifies the flowing behavior while their large values (*De*, *Ds* >>1) corresponds to solid-like behavior. Moreover, opposite trend of the velocity profile is noted for the positive values of *De* and *Ds*. Fig. 8 portrays the effects of magnetic field *M* on the velocity profile. We have seen that there is inverse relation between magnetic parameter and fluid's velocity. Fig. 9 provides the temperature profiles for different magnitudes of magnetic parameter *M*. It is noticed that temperature and thermal boundary layer thickness improves for larger magnetic parameter *M*. In fact, magnetic parameter relies on Lorentz force. As magnetic force increases, stronger the Lorentz force is and that create development in temperature and its boundary layer thickness. In Fig. 10 influence of internal heat generation/absorption parameter *hs* on temperature profile is displayed. Note that *hs* < 0 corresponds to the heat absorption phenomena while *hs* > 0 represents the heat generation situation. It is observed that the temperature and its associated boundary layer is decreasing function of heat absorption coefficient whereas an increase in temperature is noticed for the case of heat generation. Variation in temperature profile for different values of Biot number γ_1 are sketched in Fig. 11. Here temperature and thermal boundary layer thickness show an increasing behavior for large values of γ_1. Fig. 12 portrays the three-dimensional flow configuration of the considered analysis. This plots clearly shows that maximum variation is near the moving wall where decays slowly and tend to uniform free stream. Tables 1 and 2 are prepared to present the numerical magnitudes of local skin friction and local Nusselt numbers against several rheological parameters.

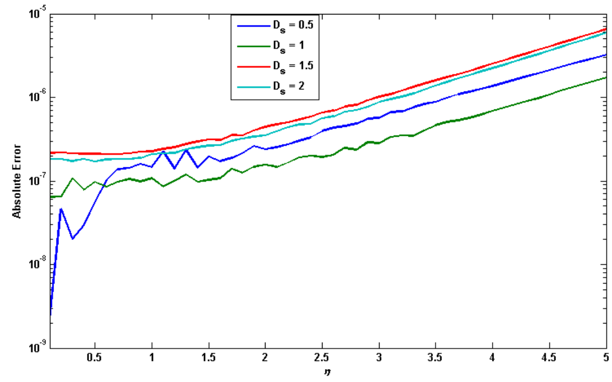

Fig. 2: Error in *f*.

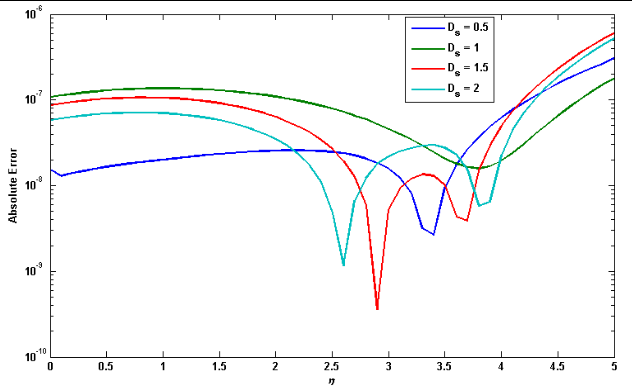

Fig. 3: Error in θ.

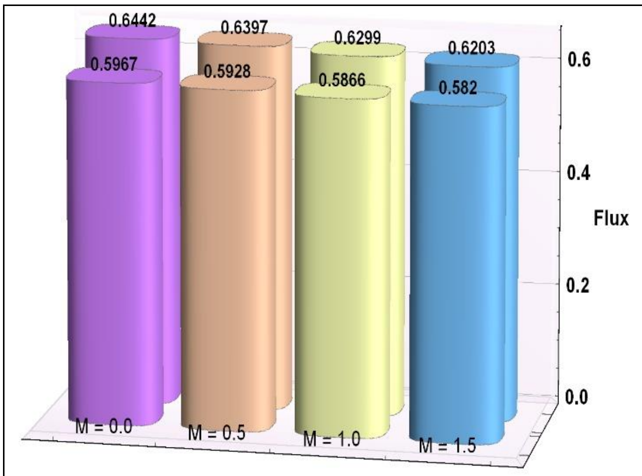

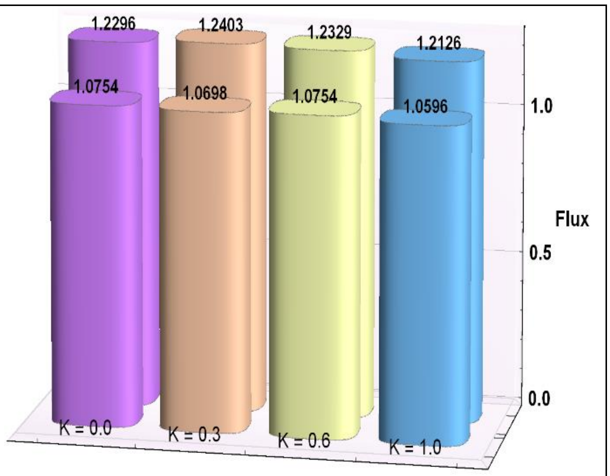

Fig. 4: Heat transfer rate against *M*. | Fig. 5: Heat transfer rate against *K*.

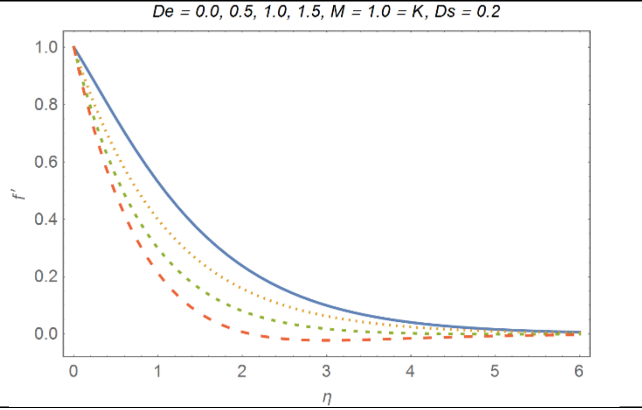

Fig. 6: Variation in *De* for f'.

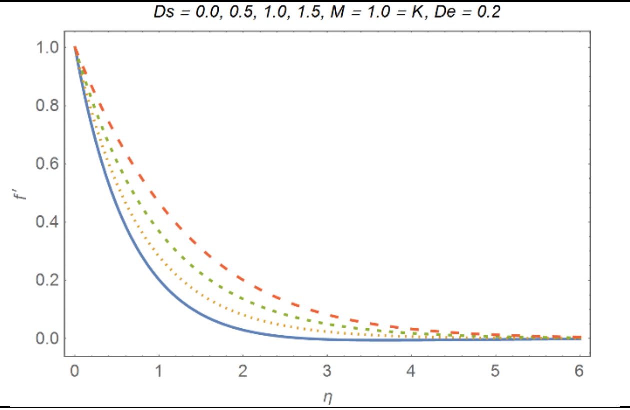

Fig. 7: Variation in *Ds* for f'.

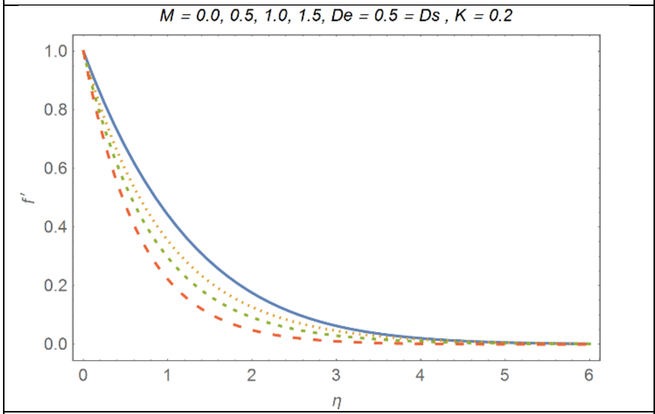

Fig. 8: Variation in *M* for f'.

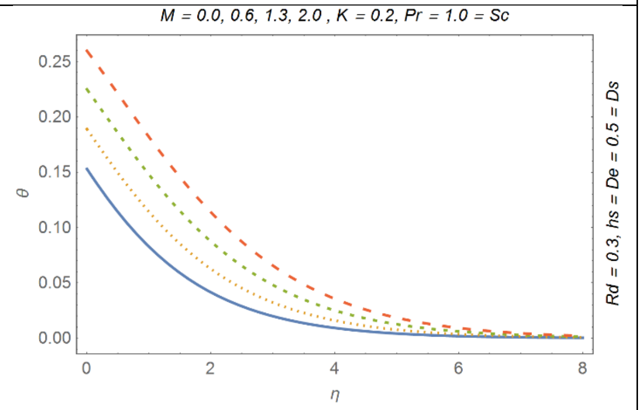

Fig. 9: Variation in *M* for θ.

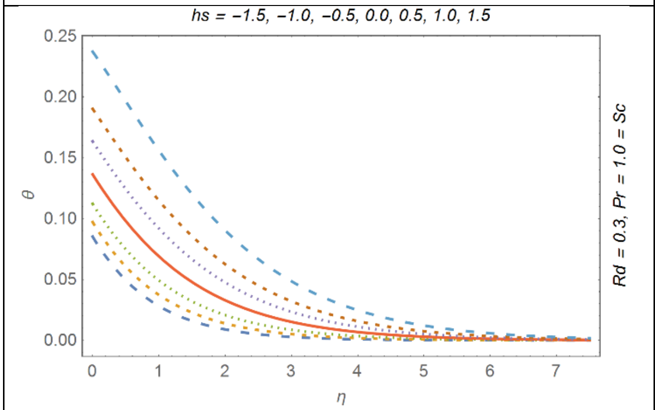

Fig. 10: Variation in *hs* for θ.

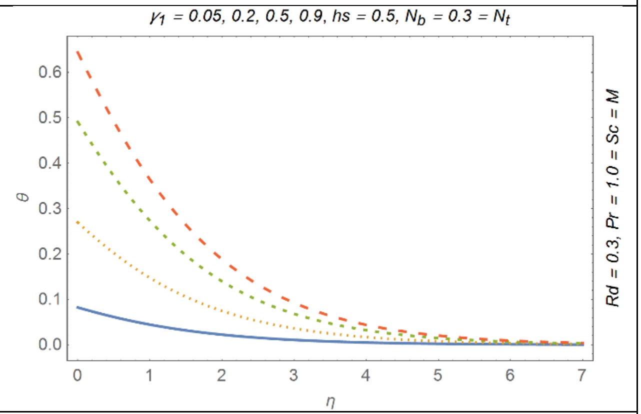

Fig. 11: Variation in γ_1 for θ.

Final outcomes

In present analysis, we examined the dynamics of Sakiadis flow of Oldroyd-B fluid over a permeable wall. Some final outcomes for present study are made on the basics of graphical results are listed below:

- Velocity and momentum boundary layers decrease for larger values of Deborah number *De* but both shows enhancement with rising values of Deborah number *Ds*.
- Magnetic field reduces the velocity of fluid.
- The temperature profile improves by increasing magnetic field.
- Opposite behaviors of heat generation and absorption effects is observed over temperature profile.
- Large values of Biot number causes increase in temperature.

In future, it looks promising to explore the potential of stochastic numerical computing methodologies [37-41] based on artificial intelligence procedures to analyze the dynamics of Sakiadis flow of Oldroyd-B fluid over a permeable wall model.

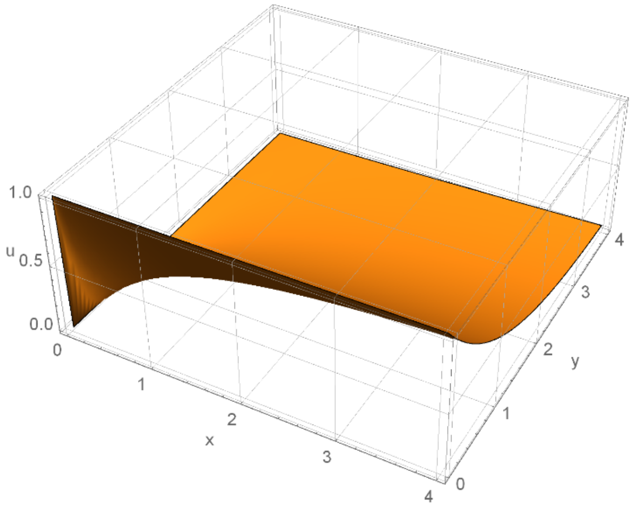

Fig. 12: Velocity plot in 3D configuration

Table 1: Numerical values of skin friction against several physical quantities.

Parameters							Numerical solutions
De	hs	M	Ds	Pr	K	γ_1	$-f''(0)$
0.0	0.5	1.0	0.5	1.0	0.5	0.5	1.91694813
0.5	0.5	1.0	0.5	1.0	0.5	0.5	1.97333087
1.0	0.5	1.0	0.5	1.0	0.5	0.5	2.03665842
1.5	0.5	1.0	0.5	1.0	0.5	0.5	2.10475407
0.5	-1.5	1.0	0.5	1.0	0.5	0.5	1.97333087
0.5	-1	1.0	0.5	1.0	0.5	0.5	1.97333087
0.5	-0.5	1.0	0.5	1.0	0.5	0.5	1.97333088
0.5	0	1.0	0.5	1.0	0.5	0.5	1.97333088
0.5	0.5	1.0	0.5	1.0	0.5	0.5	1.97333087
0.5	1.0	1.0	0.5	1.0	0.5	0.5	1.97333087
0.5	1.5	1.0	0.5	1.0	0.5	0.5	1.97480543
0.5	0.5	0.0	0.5	1.0	0.5	0.5	1.25587299
0.5	0.5	0.5	0.5	1.0	0.5	0.5	1.46704033
0.5	0.5	1.0	0.5	1.0	0.5	0.5	1.97333087
0.5	0.5	1.3	0.5	1.0	0.5	0.5	2.34576601
0.5	0.5	1.0	0	1.0	0.5	0.5	1.30360942
0.5	0.5	1.0	0.5	1.0	0.5	0.5	1.97333087
0.5	0.5	1.0	1.0	1.0	0.5	0.5	4.16623093
0.5	0.5	1.0	1.5	1.0	0.5	0.5	11.86444756
0.5	0.5	1.0	0.5	0.1	0.5	0.5	1.97333088
0.5	0.5	1.0	0.5	0.5	0.5	0.5	1.97333088
0.5	0.5	1.0	0.5	1.0	0.5	0.5	1.97333087
0.5	0.5	1.0	0.5	1.5	0.5	0.5	1.97333087
0.5	0.5	1.0	0.5	1.0	0.0	0.5	1.65264492
0.5	0.5	1.0	0.5	1.0	0.5	0.5	1.97333087
0.5	0.5	1.0	0.5	1.0	1.0	0.5	2.24931874
0.5	0.5	1.0	0.5	1.0	1.5	0.5	2.49518541
0.5	0.5	1.0	0.5	1.0	0.5	0.1	1.97333088
0.5	0.5	1.0	0.5	1.0	0.5	0.5	1.97333087
0.5	0.5	1.0	0.5	1.0	0.5	1.0	1.97333087

0.5	0.5	1.0	0.5	1.0	0.5	1.5	1.97333085

Table 2: Numerical values of wall temperature gradient against several physical quantities.

Parameters							**Numerical solutions**
De	**hs**	**M**	**Ds**	**Pr**	**K**	γ_1	$-(1+4R_d/3)\theta'(0)$
0.0	0.5	1.0	0.5	1.0	0.5	0.5	0.88626087
0.5	0.5	1.0	0.5	1.0	0.5	0.5	0.87047844
1.0	0.5	1.0	0.5	1.0	0.5	0.5	0.85857029
1.5	0.5	1.0	0.5	1.0	0.5	0.5	0.84965734
0.5	-1.5	1.0	0.5	1.0	0.5	0.5	0.47848456
0.5	-1	1.0	0.5	1.0	0.5	0.5	0.44917061
0.5	-0.5	1.0	0.5	1.0	0.5	0.5	0.39803006
0.5	0	1.0	0.5	1.0	0.5	0.5	0.25191604
0.5	0.5	1.0	0.5	1.0	0.5	0.5	0.87047844
0.5	1.0	1.0	0.5	1.0	0.5	0.5	0.35714342
0.5	1.5	1.0	0.5	1.0	0.5	0.5	0.72566043
0.5	0.5	0.0	0.5	1.0	0.5	0.5	0.96221819
0.5	0.5	0.5	0.5	1.0	0.5	0.5	0.92237457
0.5	0.5	1.0	0.5	1.0	0.5	0.5	0.87047844
0.5	0.5	1.3	0.5	1.0	0.5	0.5	0.85099774
0.5	0.5	1.0	0	1.0	0.5	0.5	−0.01897348
0.5	0.5	1.0	0.5	1.0	0.5	0.5	0.87047844
0.5	0.5	1.0	1.0	1.0	0.5	0.5	0.84028696
0.5	0.5	1.0	1.5	1.0	0.5	0.5	0.82674776
0.5	0.5	1.0	0.5	0.1	0.5	0.5	0.15693718
0.5	0.5	1.0	0.5	0.5	0.5	0.5	−0.44869951
0.5	0.5	1.0	0.5	1.0	0.5	0.5	0.87047844
0.5	0.5	1.0	0.5	1.5	0.5	0.5	0.52974335
0.5	0.5	1.0	0.5	1.0	0.0	0.5	0.21824554
0.5	0.5	1.0	0.5	1.0	0.5	0.5	0.87047844
0.5	0.5	1.0	0.5	1.0	1.0	0.5	0.85515317
0.5	0.5	1.0	0.5	1.0	1.5	0.5	0.84547170
0.5	0.5	1.0	0.5	1.0	0.5	0.1	0.14570719
0.5	0.5	1.0	0.5	1.0	0.5	0.5	0.87047844
0.5	0.5	1.0	0.5	1.0	0.5	1.0	2.30145457
0.5	0.5	1.0	0.5	1.0	0.5	1.5	5.09132362

References:

[1] Jie, P *et al.*, Characteristics of electrorheological fluid flow between two concentric cylinders. *Chinese Physics Letters*, *17 (2000),* 4, pp.298.

[2] Daniel, Y.S., *et al.*, Effects of thermal radiation, viscous and Joule heating on electrical MHD nanofluid with double stratification. *Chinese Journal of Physics*, *55 (2017)* ,3, pp.630-651.

[3] Gireesha, B.J., *et al.*,. Nonlinear convective heat and mass transfer of Oldroyd-B nanofluid over a stretching sheet in the presence of uniform heat source/sink. Results in Physics, 9(2018), pp.1555-1563.

[4] Kumar, G., *et al.*,. Thermal analysis of generalized Burgers nanofluid over a stretching sheet with nonlinear radiation and non uniform heat source/sink. Archives of Thermodynamics.(2018)

[5] Ramesh, G.K. and Gireesha, B.J.,Influence of heat source/sink on a Maxwell fluid over a stretching surface with convective boundary condition in the presence of nanoparticles. Ain Shams Engineering Journal, 5(2014), 3,pp.991-998.

[6] Colangelo, G., *et al.*, 2017. Cooling of electronic devices: Nanofluids contribution. *Applied Thermal Engineering*, *127*, pp.421-435.

[7] Gusain, R. and Khatri, O.P., Ultrasound assisted shape regulation of CuO nanorods in ionic liquids and their use as energy efficient lubricant additives. *Journal of Materials Chemistry A*, *1*(2013), 18, pp.5612-5619.

[8] B. C. Sakiadis, Boundary layer behavior on continuous solid surface I: Boundary layer equations for two dimensional and axisymmetric flow, AIChE J., 7 (1961) 26-28.

[9] B. C. Sakiadis, Boundary layer behavior on continuous solid surface II: Boundary layer on a continuous flat surface, AIChE J., 7 (1962) 221-225.

[10] J. Zierep and C. Fetecau, Energetic balance for the Rayleigh--Stokes problem of a Maxwell fluid, Int. J. Engng. Sci., 45 (2007) 617-627.

[11] M. Jamil, *et al*.,, Unsteady helical flows of Oldroyd-B fluids, Comm. Nonlinear Sci. Numer. Simulat., 16 (2011) 1378-1386.

[12] W. Tan and T. Masuoka, Stability analysis of a Maxwell fluid in a porous medium heated from below, Phys. Letters A, 360 (2007) 454-460.

[13] S. Nadeem, *et al*., HAM solutions for boundary layer flow in the region of the stagnation point towards a stretching sheet, Comm. Nonlinear Sci. Numer. Simulat., 15 (2010) 475-481.

[14] T. Hayat, A. Alsaedi, On thermal radiation and Joule heating effects on MHD flow of an Oldroyd-B fluid with thermophoresis. Arb. J. Sci. Eng. **36**(2011) 1113–1124.

[15] M. Y. Malik, *et al*.,, Magnetohydrodynamic three-dimensional Maxwell fluid flow towards a horizontal stretched surface with convective wall, Int. J. BioEngng. Life Sci., 2 (2015).

[16] T. Hayat, *et al*.,, Mixed convection three-dimensional flow of an upper-convected Maxwell (UCM) Fluid under magnetic field, thermal-diffusion and diffuion-thermo effects, ASME, J. Heat Transfer, 134 (2012) 044503.

[17] Mehmood, Z., *et al*.,, 2017. Numerical investigation of micropolar Casson fluid over a stretching sheet with internal heating. Communications in Theoretical Physics, 67(2017),4, p.443.

[18] Ramesh, G.K. and Gireesha, B.J.,Influence of heat source/sink on a Maxwell fluid over a stretching surface with convective boundary condition in the presence of nanoparticles. Ain Shams Engineering Journal, 5(2014), 3,pp.991-998.

[19] Mehmood, R., *et al*.,Flow and heat transfer analysis of Jeffery nano fluid impinging obliquely over a stretched plate. Journal of the Taiwan Institute of Chemical Engineers, 74(2017) , pp.49-58.

[20] Kumar, K.G., *et al*.,. Characteristics of Joule heating and viscous dissipation on three-dimensional flow of Oldroyd B nanofluid with thermal radiation. Alexandria Engineering Journal.(2017)

[21] Rana, S., *et al*.,.Free convective nonaligned non-Newtonian flow with non-linear thermal radiation. Communications in Theoretical Physics, 66(2016), 6, p.687.

[22] Awais, M., *et al*.,. Generalized magnetic effects in a Sakiadis flow of polymeric nano-liquids: Analytic and numerical solutions. Journal of Molecular Liquids. 241 (2017), pp 570-576.

[23] Ahmed, N., *et al.*, 2018. A theoretical investigation of unsteady thermally stratified flow of γAl2O3− H2O and γAl2O3− C2H6O2 nanofluids through a thin slit. *Journal of Physics and Chemistry of Solids (2018)*.

[24] Phule, A.D., *et al*.,Negative optical absorption and up-energy conversion in dendrites of nanostructured silver grafted with α/β-poly (vinylidene fluoride) in small hierarchical structures. *Journal of Physics and Chemistry of Solids*, *115 (2018)*, pp.254-264.

[25] Rana, S., *et al*.,. Mixed convective oblique flow of a Casson fluid with partial slip, internal heating and homogeneous–heterogeneous reactions. Journal of Molecular liquids, 222(2016), pp.1010-1019.

[26] Iqbal, Z *et al*.,. Impact of inclined magnetic field on micropolar Casson fluid using Keller box algorithm. The European Physical Journal Plus, 132(2017), 4,p.175.

[27] Tabassum, *et al*.,. Impact of viscosity variation and micro rotation on oblique transport of Cu-water fluid. Journal of colloid and interface science, 501(2017), pp.304-310.

[28] Awais, M., *et al*.,. Hydromagnetic mixed convective flow over a wall with variable thickness and Cattaneo-Christov heat flux model: OHAM analysis. Results Physics, 8 (2018), pp 621-627

[29] Mehmood, R., *et al*.,. Effects of transverse magnetic field on a rotating micropolar fluid between parallel plates with heat transfer. Journal of Magnetism and Magnetic Materials, 401(2016), pp.1006-1014.

[30] Rehman, A.U *et al*.,. Entropy analysis of radioactive rotating nanofluid with thermal slip. Applied Thermal Engineering, 112(2017), pp.832-840.

[31] Ramesh, G.K., *et al*., MHD mixed convection flow of a viscoelastic fluid over an inclined surface with a nonuniform heat source/sink. Canadian Journal of Physics, 91(2013),12, pp.1074-1080.

[32] T. Hayat, *et al*.,, Similar solution for three-dimensional flow in an Oldroyd-B fluid over a stretching Surface, International Journal for Numerical Methods in Fluids, 70 (2012) 851-859.

[33] Awais, *et al*., Nanoparticles and nonlinear thermal radiation properties in the rheology of polymeric material. *Results in Physics*, *8(2018)*, pp.1038-1045.

[34] Awan, S.E., *et al*., 2018. Dynamical analysis for nanofluid slip rheology with thermal radiation, heat generation/absorption and convective wall properties. AIP Advances, 8(2018),7, p.075122.

[35] Siddiqa, S., *et al*., 2018. Thermal radiation therapy of biomagnetic fluid flow in the presence of localized magnetic field. International Journal of Thermal Sciences, 132, pp.457-465.

[36] Awan, S.E., *et al*.,Numerical Treatment for Hydro-magnetic Unsteady Channel Flow of Nanofluid with Heat Transfer. Results in Physics. 9(2018) ,pp. 1543-1554.

[37] Mehmood, A., *et al*., Intelligent computing to analyze the dynamics of Magnetohydrodynamic flow over stretchable rotating disk model. *Applied Soft Computing*, *6(2018) 7*, pp.8-28.

[38] Raja, M.A.Z., *et al*.,. Intelligent computing strategy to analyze the dynamics of convective heat transfer in MHD slip flow over stretching surface involving carbon nanotubes. *Journal of the Taiwan Institute of Chemical Engineers*, *8(2017)* , pp.935-953.

[39] Raja, M.A.Z., *et al*.,. Bio-inspired computational heuristics to study the boundary layer flow of the Falkner-Scan system with mass transfer and wall stretching. *Applied Soft Computing*, *57(2017)*, pp.293-314.

[40] Raja, M.A.Z., *et al*.,. Design of bio-inspired computing technique for nanofluidics based on nonlinear Jeffery–Hamel flow equations. *Canadian Journal of Physics*, *94*(2016), 5, pp.474-489.

[41] Raja, M.A.Z., Manzar, M.A., Shah, F.H. and Shah, F.H., 2018. Intelligent computing for Mathieu’s systems for parameter excitation, vertically driven pendulum and dusty plasma models. *Applied Soft Computing*, *62*, pp.359-372.